



Information-Theoretic Active Polygons for Unsupervised Texture Segmentation

GOZDE UNAL

Siemens Corporate Research, Princeton, NJ 08540

gozde.unal@siemens.com

ANTHONY YEZZI*

School of ECE, Georgia Tech., Atlanta, GA 30332

ayezzi@ece.gatech.edu

HAMID KRIM†

Department of ECE, NCSU, Raleigh, NC 27695

ahk@eos.ncsu.edu

Received June 20, 2002; Revised May 17, 2004; Accepted May 21, 2004

First online version published in November, 2004

Abstract. Curve evolution models used in image segmentation and based on image region information usually utilize simple statistics such as means and variances, hence can not account for higher order nature of the textural characteristics of image regions. In addition, the object delineation by active contour methods, results in a contour representation which still requires a substantial amount of data to be stored for subsequent multimedia applications such as visual information retrieval from databases. Polygonal approximations of the extracted continuous curves are required to reduce the amount of data since polygons are powerful approximators of shapes for use in later recognition stages such as shape matching and coding. The key contribution of this paper is the development of a new active contour model which nicely ties the desirable polygonal representation of an object directly to the image segmentation process. This model can robustly capture texture boundaries by way of higher-order statistics of the data and using an information-theoretic measure and with its nature of the ordinary differential equations. This new variational texture segmentation model, is unsupervised since no prior knowledge on the textural properties of image regions is used. Another contribution in this sequel is a new polygon regularizer algorithm which uses electrostatics principles. This is a global regularizer and is more consistent than a local polygon regularization in preserving local features such as corners.

Keywords: region-based active contours, unsupervised segmentation, texture segmentation, polygon evolution, information theoretic measure, electrostatic regularizer

1. Introduction

Image segmentation is generally viewed as an essential first step in low level vision and as providing a mechanism for an automatic analysis of image contents. Snakes (Kass et al., 1988) and active contour

*Supported by NSF grant CCR-0133736.

†Partially supported by AFOSR grant F49620-98-1-0190 and NSF grant CCR-9984067.

methods define energy functionals whose local minima include boundaries of image regions. The two main streams of thought emerged in active contours. Geometric active contour models (Kichenassamy et al., 1995; Caselles et al., 1995, 1993; Malladi et al., 1995; Siddiqi et al., 1998), were developed as gradient flows of a modified Euclidean arc length which has almost zero weight near edges, and larger weight far from them. These models are hence edge-based, and are only sensitive to data near the curve, are hence prone to noise variability and to initial contour placement. To overcome this problem, region-based active contours, which use both local and global information were proposed (Chan and Vese, 1999; Yezzi et al., 1999; Ronfard, 1994; Zhu and Yuille, 1996; Chakraborty et al., 1996). These models mainly assume that the image consists of a finite number of regions, that are characterized by a pre-determined set of features or statistics such as means, and variances. An energy functional is constructed to pull these statistics apart. One advantage over the geometric active contours is that there is no need to calculate image gradients which are usually sensitive to noise, albeit at a cost of additionally imposed assumptions on the image. The popularity of these active contour models was particularly due to an efficient implementation scheme via partial differential equations (PDEs), referred to as level set methods (Osher and Sethian, 1988; Sethian, 1999).

Global optimization approaches to image segmentation are based on energy functions minimizing different criteria such as Minimum Description Length (MDL) (Leclerc, 1989), and Bayesian (Blake and Zisserman, 1987), and region competition (Zhu et al., 1998). A well-known mathematical model (Mumford and Shah, 1985) sought to additionally extract a boundary by approximating an image by smooth functions in each region. Level-sets active contour implementation of this model have recently been introduced in Chan and Vese (2001) and Tsai et al. (2001).

A particularly powerful cue in visual perception is the set of textural features. Texture segmentation, which is the task of parsing the image domain into a number of regions such that each region has the same textural properties is a challenging problem (Jain and Farrokhnia, 1991; Manjunath and Chellappa, 1991). The problem of unsupervised texture segmentation, which proceeds without a priori information about the textural characteristics of objects in a given image

remains largely an active research issue in computer vision.

1.1. Related Work and Contribution

For texture analysis and modelling, two main groups of approaches (or combinations thereof) have been developed (applied): (i) Filtering techniques based on filter-banks of Gaussians and Gabor functions to characterize different attributes of a texture at different orientations and scales (Jain and Farrokhnia, 1991; Simoncelli et al., 1992) have been shown to be efficient at capturing local spatial features. Note, however, that problems such as optimal choices of filters, and fusion of their outputs remain open. (ii) Statistical modelling approaches characterize texture images as arising from probability distributions on Markov Random Fields (MRF's) (Manjunath and Chellappa, 1991; Besag, 1973; Geman and Geman, 1984; Cross and Jain, 1983), and their segmentation is achieved through a minimization of a maximum a posteriori (MAP) criterion of the observed image. An advantage of these approaches is that they yield the parameters of the underlying probability distribution which in turn, affords one an ability to synthesize texture images by sampling. Limitations of commonly used MRF models, on the other hand, are due to the fact that only the first and second order statistics may tractably be used, while, it is widely recognized that many textures are strongly non-Gaussian regardless of the neighborhood size (Zhu et al., 1998). An analytical probability density for modeling clutter in natural images was proposed in Grenander and Srivastava (2001).

Methods which attempt to unify the aforementioned approaches have recently received attention. Zhu and Yuille's region competition model (Zhu and Yuille, 1996) in texture segmentation used two local orientations of texture elements obtained through a Gaussian filtering of image gradient components as multivariate texture images. Zhu et al. (1998) developed a maximum entropy probability model built on the texture features extracted by a set of filters aimed at also capturing the properties of the texture at multiple scales and orientations. More detailed than classical MRF's, these models are better able to capture non-Gaussian textures. We, however, note that in contrast to our interest herein, namely in texture segmentation, their main goal is texture synthesis. The heavy computational burden, which we aim to avoid, is an additional issue which sets our proposed approach

apart from the afore-cited technique. Paragios and Deriche (2002) also combined a filtering approach with a statistical view while accounting for boundary-based and region-based active contour frameworks, to capture texture boundaries. This method requires a prior knowledge on the existing textures in the given image, to estimate a Gaussian mixture probability distribution representing these pre-defined textures.

Our overall objective of object (homogeneous region) delineation in an observed image is highly motivated by classification and recognition applications. This in turn, and in contrast to existing active contours, motivates a parsimonious and revealing representation such as that based on landmarks/vertices of an approximating polygon as we propose in this paper. In addition to its parsimony, this representation is expected to accurately capture the prevailing texture and account for it in the course of the analysis.

To motivate our investigation, an example of a synthetic image of two distinct intensity regions with additive uniform noise is illustrated in Fig. 1. Most active contour models require significant regularization on the contour in the presence of noise in the image. With little regularization, the curve weaves around noise, with medium regularization, there is still no way for an active contour to get out of local minima in this highly noisy case. With a very large regularization, the curve starts to converge to the shape, but the shrinking effect is too powerful, and the curve continues to shrink without sticking to the data, and eventually will collapse to a point. By evolving an active polygon with a relatively small number of vertices, strong regularizing internal forces are no longer necessary to keep the contour from “breaking-up”. A polygon laid on the same noisy image in Fig. 1, propagates towards the boundaries with a greater resilience to noise, and results in

a good delineation of the target object with only four vertices accurately located at the corners of the object. While our introduced model is applied to a seemingly contrived simple example, it nevertheless, illustrates the propagation of an active polygon through noise, and free of cost due to sharp corners.

We propose a new texture segmentation approach which utilizes an information-theoretic measure, namely Jensen-Shannon divergence, which to our knowledge has not been used in the active contour framework, and seeks to distinguish and separate probability density functions of various regions in an image. This measure makes use of higher order statistics beyond mean and variance by a computationally efficient manner which does not require histograms. Jensen-Shannon divergence (Lin, 1991; He et al., 2003), with Shannon entropy as a specific case (Cover and Thomas, 1991), is a probabilistic difference measure, with properties of interest in various applications. For instance, unlike most other divergence measures, it can be generalized to a finite number of probability distributions, which makes it suitable to an image segmentation scenario with several target regions. For an image registration application, a similar divergence measure, based on a Renyi entropy (Cover and Thomas, 1991), was proposed by He et al. (2003), and referred to as a Jensen-Renyi divergence. Jensen-Shannon divergence was also applied to edge detection on regular or texture images in Gomez-Lopera et al. (2000) by measuring the probabilistic differences between relative frequency of gray values in two halves of a small window that is slid over an image. Since it was developed for edge detection purposes, the result of this method yields unconnected edges, and contours, and requires further processing such as contour linking for a segmentation purpose. It hence differs

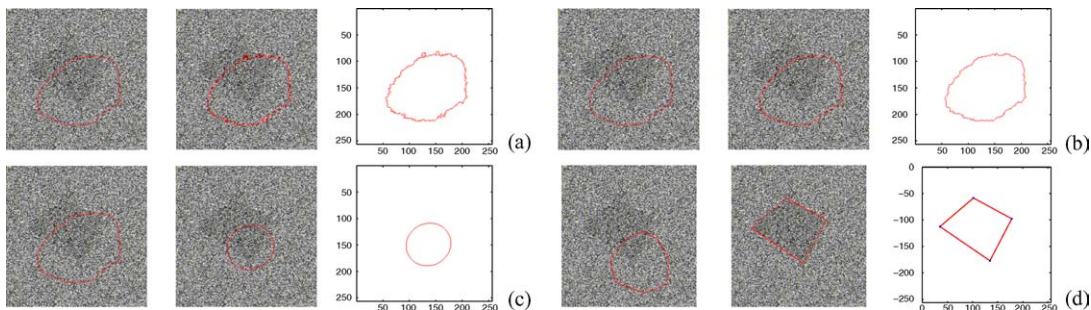


Figure 1. A simple image of a quadrilateral with additive uniform noise is segmented by: an continuous active contour propagation with (a) small, (b) medium, (c) large regularization; (d) an active polygon.

from our approach which aims at finding a solid segmentation of objects in an image within a variational framework. Our technique does not assume an underlying Gaussian model for texture regions, in contrast to Zhu and Yuille (1996), and is hence statistically non-parametric, and image data drives the estimation of the divergence between the texture distributions. In contrast to our approach (Chesnaud et al., 1999), assume particular prior densities which have explicit expressions, and then make use of a MAP criterion minimized by an iterative stochastic optimization via a polygon.

In our approach, the formulation of such an energy functional in conjunction with a polygonal probing tool, is followed by a gradient-based minimization procedure which evolves the vertices by way of a coupled set of Ordinary Differential Equations (ODEs). To prevent degeneracy during motion of the vertices (e.g. edges intersecting each other), we propose a global regularizer technique which uses electrostatics principles by viewing each edge of the polygon as a line of uniform charge. This particular point is also of interest in its own right, as it introduces a globally geometric regularizer rather than local geometric regularizers that have been popular.

Remark. While technically conventional discrete particle based implementations of active contours (even going back to the snake model of Kass et al.) may be considered polygonal models, there is a key difference, both philosophically and numerically, between these more conventional “active contours” implemented discretely as finely sampled polygons and what we are calling “active polygons”. This difference is that conventional discrete implementations of active contours are point-wise in their treatment of the model. Namely, forces derived from image measurements for evolving each vertex are obtained only in the vicinity of that particular vertex. In our case, however, the basic element of the discrete model is no longer the vertex but instead the edges between vertices along which image information is “accumulated” in order to determine the motion of the vertex. This changes both the mathematical treatment of the model as well as its numerics. In conventional snakes, it is desirable to have very closely spaced vertices since many sample points are needed to approximate the underlying “non-polygonal” model (otherwise very little image information will be used) whereas in an “active polygon” it is desirable to have very few vertices in order to

yield longer edges (which in turn allow for more averaging of image information along such edges). Rather than marker-particle based techniques, our approach is philosophically much more related to, but nevertheless quite different from, spline-based models, where the entire contour is represented by a few control points, such as Blake and Isard (1998), Cremers et al. (2002) and Figueiredo et al. (2000). The approach we propose aims at an unsupervised texture segmentation scenario, in which the only prior information is the number of different classes/regions which are assumed to be simply connected due to our simple ODEs.

1.2. *Discussion on Active Polygons vs. Active Contours*

Active polygons enjoy some advantages and flexibility over existing techniques:

- The system of ODEs which results from our formulation turns local image measurements at points on the contour into global information, as these local measurements are integrated along the polygon edges. This makes our algorithm much more reliable and robust at capturing texture boundaries in contrast to continuous curves which are local in scope. Region-based methods also use global information inside and outside the curve, but their gradient flow incorporates local information, and point-wise on the curve, and is hence not amenable to speed functions for capturing higher-order statistics which can not be estimated from pointwise measurements.
- A reliable detection of sharp object corners is particularly important in recognition and classification of man-made objects. The algorithm presented introduces no rounding effects at such important feature points, which sets it apart from the continuous approaches. Furthermore, content based description of multimedia data entails a demand for an efficient access and representation of visual objects in a scene. An efficient description of an object is its contour representation, which may still require a considerable amount of information to be stored. The goal is often to reduce the amount of data (e.g. complex figures in cartography, geographical maps), and polygons are powerful approximators of shapes (Dunham, 1986; Kurozumi and Davis, 1982; Imai and Iri, 1986; Freeman, 1978) for use in later recognition stages (Koch and Kashyap, 1987), such as

shape matching, and shape coding. Several techniques for shape coding such as O'Connell (1997) and Yun et al. (2001), entailed first extracting object boundaries and subsequently finding a polygonal approximation of the extracted contour. With a goal of efficient compression, our technique, is hence advantageous in that it captures in one shot, a polygonal representation of objects in an image, while avoiding a typically lengthy search for meaningful locations, such as high curvature points, used in shape matching. The polygonal representation of an object from an image is only as good as the segmentation of the image. It is thus more efficient to invoke the polygonal representation directly in the course of the image segmentation process rather than afterwards. In short, our approach connects the final polygonal representation we wish to use, directly to the image data.

- Another advantage of using ODEs rather than PDEs is a more efficient implementation. In the discretization, a significantly larger time step can be chosen to speed up the algorithm, whereas the PDEs usually require very small time steps for stable numerical implementations, particularly when strong regularizers, which are avoided by our model, are necessary.
- A particularly interesting property of the proposed approach is that a stochastic component may easily be incorporated, contrary to the continuous curve propagation by PDEs. One can indeed add a random perturbation component to the deterministic ODE component, such as a standard Brownian motion with a certain variance, in order to make the evolution more robust to noise effects and, usually yielding a convergence to a local extremum of the objective functional.
- Finally, we incorporate a novel global regularizer to the vertex motion equations using electrostatics principles. When the regularizer is the sole term acting on the polygon, it forces the polygonal edges and vertices to remain apart as imposed by the electric field induced at a vertex. We note that our proposed approach is to be distinguished from that of Bruckstein et al. (1995), which, using a discrete form of curvature to account for only local geometry, evolves a polygon in the absence of an image term, and with a different intended application. Our global, rather than local, regularizer is more consistent in preserving local features such as corners.

The paper is organized as follows. In the next section, we derive the ODEs to obtain motion equations for polygon vertices. In Section 3, we introduce the Jensen-Shannon criterion for evolving a single contour and multiple contours with the goal of texture segmentation. In Section 4, a novel polygon regularizer is introduced in order to avoid degeneracy in the course of the polygon propagation. To our knowledge, this type of global geometric regularizer has been used nowhere, including all related spline-based active contour models. Results, conclusions and discussions are given in Section 5.

2. Active Polygons

The dynamical equation of an active contour, typically follows the construction of an energy functional around a region which is subsequently minimized by a gradient descent flow. Our goal is to design flows to move a polygon by its relatively small number of vertices rather than a continuous active contour. To explicitly invoke a contour $C : [a, b] \subset \mathbb{R} \rightarrow \mathbb{R}^2$ around some region $R \subset \mathbb{R}^2$, in which the integrand $f(x, y)$ consists of a function $f : \mathbb{R}^2 \rightarrow \mathbb{R}$, we use the divergence theorem to write an integral over the interior of a curve as a contour integral

$$E(C) = \iint_R f(x, y) dx dy = \oint_{C=\partial R} \langle \mathbf{F}, \mathbf{N} \rangle ds,$$

where \mathbf{N} denotes the outward unit normal to C , ds the Euclidean arclength element, and where $\mathbf{F} = (F^1, F^2)$ is chosen so that $\nabla \cdot \mathbf{F} = f$. In what follows we will let $p \in [a, b]$ denote a fixed parameterization of the curve where $C(a) = C(b)$. We will indicate by v any variable whose variation affects the geometry of the curve. In the case of a polygon, v will denote a Cartesian coordinate of any vertex. In the case of a smooth curve, v will denote a curvilinear coordinate which varies along the normal direction at any point on the curve but remains constant along the curve itself. The key point, in either case, is that v and p constitute independent variables. We now rewrite the contour integral in terms of the parameter p ,

$$E(C) = \int_a^b \langle \mathbf{F}, \mathbf{N} \rangle \|C_p\| dp = \int_a^b \langle \mathbf{F}, \mathbf{J}C_p \rangle dp,$$

where

$$\mathbf{J} = \begin{bmatrix} 0 & 1 \\ -1 & 0 \end{bmatrix}, \quad \text{and} \quad \mathbf{N}\|\mathbf{C}_p\| = \mathbf{J}\mathbf{C}_p.$$

In order to determine the gradient flow associated with E , we compute the derivative with respect to v . After some manipulations, E_v can be obtained as Zhu and Yuille (1996) and Yezzi et al. (2002)

$$E_v(\mathbf{C}) = \int_a^b f(\mathbf{C}_v, \mathbf{J}\mathbf{C}_p) dp. \quad (1)$$

In the case of a smooth curve \mathbf{C} , the variable v denotes, at each point on the curve, a coordinate which varies in the normal direction to the curve. Thus, if we are considering geometric evolutions $\frac{\partial \mathbf{C}}{\partial t}$ of the curve, we see from the final expression of E_v , that the gradient flow for \mathbf{C} with respect to E is given by

$$\frac{\partial \mathbf{C}}{\partial t} = f\mathbf{N}. \quad (2)$$

Proceeding along a similar but slightly modified line of thought, we consider a closed polygon \mathbf{V} as the contour \mathbf{C} , and with a fixed number of vertices $\{\mathbf{V}_1, \dots, \mathbf{V}_n\} = \{(x_i, y_i), i = 1, \dots, n\}$. We may parameterize \mathbf{C} by $p \in [0, n]$ as

$$\mathbf{C}(p, \mathbf{V}) = L(p - \lfloor p \rfloor, \mathbf{V}_{\lfloor p \rfloor}, \mathbf{V}_{\lfloor p \rfloor + 1}) \quad (3)$$

where $\lfloor p \rfloor$ denotes the largest integer which is not greater than p , and where $L(t, \mathbf{A}, \mathbf{B}) = (1-t)\mathbf{A} + t\mathbf{B}$ parameterizes between 0 to 1 the line from \mathbf{A} to \mathbf{B} with constant speed, (\mathbf{A} and \mathbf{B} denote the end points of a polygon edge). Note that the indices of \mathbf{V} should be interpreted as modulo n so that \mathbf{V}_0 and \mathbf{V}_n denote the same vertex (recall \mathbf{C} is a closed curve). Finally, note that \mathbf{C}_p is defined almost everywhere (where $p \neq \lfloor p \rfloor$) by

$$\mathbf{C}_p(p, \mathbf{V}) = \mathbf{V}_{\lfloor p \rfloor + 1} - \mathbf{V}_{\lfloor p \rfloor}. \quad (4)$$

Proposition 1. *Using the above parameterization $\mathbf{C}_p(p, \mathbf{V})$ in Eq. (1), we obtain the first variation of the energy functional E as*

$$E_v = \int_0^n f(L(p - \lfloor p \rfloor, \mathbf{V}_{\lfloor p \rfloor}, \mathbf{V}_{\lfloor p \rfloor + 1})) \times \langle \mathbf{C}_v, \mathbf{J}(\mathbf{V}_{\lfloor p \rfloor + 1} - \mathbf{V}_{\lfloor p \rfloor}) \rangle dp, \quad (5)$$

and the minimization of E is achieved by a gradient descent flow given by a set of ODEs for each vertex $\mathbf{V}_k, k = 1, \dots, n$, as (see Appendix A)

$$\begin{aligned} \frac{\partial \mathbf{V}_k}{\partial t} = & \int_0^1 pf(L(p, \mathbf{V}_{k-1}, \mathbf{V}_k)) dp \mathbf{N}_{k,k-1} \\ & + \int_0^1 (1-p)f(L(p, \mathbf{V}_k, \mathbf{V}_{k+1})) dp \mathbf{N}_{k+1,k}, \end{aligned} \quad (6)$$

where $\mathbf{N}_{k,k-1}$ (resp. $\mathbf{N}_{k+1,k}$) denotes the outward unit normal of edge $(\mathbf{V}_{k-1} - \mathbf{V}_k)$ (resp. $(\mathbf{V}_k - \mathbf{V}_{k+1})$).

Written for each vertex, these equations are a set of coupled ordinary differential equations to be simultaneously solved. Intuitively, any of these equations concisely re-written as

$$\frac{\partial \mathbf{V}_k}{\partial t} = \tilde{f}_{k,k-1} \mathbf{N}_{k,k-1} + \tilde{f}_{k+1,k} \mathbf{N}_{k+1,k} \quad (7)$$

integrates the information, which is obtained from image values along two adjacent edges $(\mathbf{V}_{k-1} - \mathbf{V}_k)$, and $(\mathbf{V}_k - \mathbf{V}_{k+1})$, and combined with the global image statistics (depending on the function f), into two overall speed functions $\tilde{f}_{k,k-1}$, and $\tilde{f}_{k+1,k}$ in order to move the vertex \mathbf{V}_k . This system of ODEs hence effectively implements a coupled motion of all the vertices of a polygon. In addition, this integration procedure, provides improved robustness to noise. Another advantage of the flow in Eq. (6) is the reduction of the dimension of contour propagation problem from a theoretically infinite one to roughly on the order of 3–30 vertex points, depending on the complexity of an object boundary. This also clearly highlights the differences mentioned earlier between active polygons and marker particle methods. One may note the significantly reduced number of well separated vertices which have to be propagated. In addition, the motion of each vertex being based on a weighted combination of the unit normals only at the polygon's edge points, implies that there is no need for a unit normal to be defined at a vertex. As a result, the polygonal contour formed by these vertex locations $(\mathbf{V}_1, \dots, \mathbf{V}_n)$ need not be differentiable. A generic image-based term, indeed a speed function f , can be used in the derived ODEs describing the motion of our active polygons, hence making them quite flexible.

For illustration, we apply our active polygon model in Eq. (6) to an image using simple mean statistics for the foreground and the background. In Fig. 2, an



Figure 2. Demonstration of flow (6).

active polygon is propagated where its edges align themselves along the edges of the target object, which is a simple triangle shape, with the influence of the weights determined by the data term. The result of the polygon propagation shown at the right is automatically the location of 3 vertices of the target triangle. Implementation issues along with the initialization are discussed in Section 5.1.

3. An Information-Theoretic Criterion

It is commonly assumed in region-based active contours that an image is piecewise constant. Several techniques based on utilizing the first and second order statistics have been proposed. While these techniques are quite adequate for Gaussian data, they are highly insufficient to capture the underlying information in non-Gaussian data which include almost all textures. Towards that end, we use an information theoretic measure which not only captures the higher order information of non-Gaussian data, but provides a probabilistic disparity measure among N data populations. Hence, we consider a decision problem with N classes c_1, \dots, c_N with prior probabilities, $\mathbf{a} = (a_1, \dots, a_N)$ such that $\sum_{i=1}^N a_i = 1$. Based on the Shannon entropy H , the so-called generalized Jensen-Shannon divergence (Lin, 1991; He et al., 2003) among N probability densities is

$$JS_a = H\left(\sum_{i=1}^N a_i p_i(\xi)\right) - \sum_{i=1}^N a_i H(p_i(\xi)) \quad (8)$$

where $p_i(\xi)$ denotes the probability density of the i th class in a region. One of the major features of the Jensen-Shannon divergence is that different weights a_i may be assigned to the relevant distributions according to their importance.

Our ability to better capture the underlying statistics of regions using the entropy-based symmetric divergence measure, suggests that this may play a key role in constructing an energy functional whose optimization would yield a polygonal flow to well delineate differently textured regions. To proceed, and for the sake of efficiency, we resort to a fast numerical estimation of the densities which in turn facilitates the estimation of the entropies and hence of the divergence measure. We chose to adopt a first order approximation of a density which achieves the maximum entropy solution, and which, in turn, is used in approximating the entropy expression as proposed by Hyvarinen (1997).

On a region delineated by an active contour, we assume a scalar random variable (r.v.) ξ on a given set of intensity values Ξ , $\xi : \Xi \subset \mathbb{R} \rightarrow \mathbb{R}^+$, and the available information on the density of the r.v. ξ is given by

$$\int_{\Xi} p(\xi) G_j(\xi) d\xi = u_j, \quad \text{for } j = 1, \dots, m, \quad (9)$$

where the estimates u_j are the expectations $E\{G_j(\xi)\}$ of m known independent functions $\{G_j(\cdot)\}$ of ξ . Note that there is no model assumption for the random variable ξ , however, the distribution which has the maximum entropy and which is also compatible with the measurements in Eq. (9) is sought (Cover and Thomas, 1991; Jaynes, 1963). This problem has been widely studied, and the form of the maximum entropy distribution has been derived in Cover and Thomas (1991) and Jaynes (1963). The density $p_o(\xi)$ which satisfies the constraints (9) and has maximum entropy among all such densities is of the form $p_o(\xi) = B e^{\sum_{j=1}^m b_j G_j(\xi)}$ where B and b_j are constants that are determined from the constraints. A first order approximation for this maximum entropy density denoted by $\hat{p}(\xi)$, is given

by Hyvarinen (1997)

$$\hat{p}(\xi) = \phi(\xi) \left(1 + \sum_{j=1}^m u_j G_j(\xi) \right) \quad (10)$$

where $u_j = E\{G_j(\xi)\}$, and $\phi(\xi)$ is the standard Gaussian density $\phi(\xi) = \exp(-\xi^2/2)/\sqrt{2\pi}$. ($E\{\cdot\}$ is the expectation of a random variable). In practice, the u_j 's are estimated as the corresponding sample averages of the $G_j(\xi)$, i.e. we compute measurements in a region R of an image function $I: \mathbb{R}^2 \rightarrow \mathbb{R}$ by $u_j = \frac{1}{|R|} \sum_{(x,y) \in R} G_j(I(x,y))$, where $|R|$ is the number of pixels in R . A simple approximation of the entropy functional is subsequently found upon substituting the approximate density $\hat{p}(\xi)$ in

$$H(\hat{p}(\xi)) = - \int_{\Xi} \hat{p}(\xi) \log \hat{p}(\xi) d\xi \approx H(v) - \frac{1}{2} \sum_{j=1}^m u_j^2, \quad (11)$$

where $H(v) = \frac{1}{2}(1 + \log(2\pi))$ is the entropy of a standardized Gaussian variable (see (Hyvarinen, 1997) for details). This result implies that a first order approximate maximum entropy of a given distribution is found by calculating how far away it is from that of the standard Gaussian density.

3.1. Evolution of a Single Active Contour

With a single contour, the image domain $\Omega \subset \mathbb{R}^2$ is split into two regions, namely a region inside the contour, call it R_u , and a region outside the contour, $\Omega \setminus R_u$. Exploiting the approximation in Eq. (11), we define an energy functional whose optimization yields the evolution of our active contour based on a divergence measure defined in Eq. (8). The new energy functional for two regions, is

$$\begin{aligned} JS_{a,2} &= H(a_1 \hat{p}_1(\xi) + a_2 \hat{p}_2(\xi)) \\ &\quad - a_1 H(\hat{p}_1(\xi)) - a_2 H(\hat{p}_2(\xi)) \\ &= - \int_{\Xi} (a_1 \hat{p}_1(\xi) + a_2 \hat{p}_2(\xi)) \log(a_1 \hat{p}_1(\xi) \\ &\quad + a_2 \hat{p}_2(\xi)) d\xi + a_1 \int_{\Xi} \hat{p}_1(\xi) \log(\hat{p}_1(\xi)) d\xi \\ &\quad + a_2 \int_{\Xi} \hat{p}_2(\xi) \log(\hat{p}_2(\xi)) d\xi, \end{aligned} \quad (12)$$

Here the expression $H(a_1 \hat{p}_1(\xi) + a_2 \hat{p}_2(\xi))$ may similarly to $H(p_1(\xi))$ be approximated by substituting the

approximate density expression in Eq. (10) to yield

$$\begin{aligned} &H(a_1 \hat{p}_1(\xi) + a_2 \hat{p}_2(\xi)) \\ &\approx - \int_{\Xi} \left(a_1 \phi(\xi) \left[1 + \sum_{j=1}^m u_j G_j(\xi) \right] \right. \\ &\quad \left. + a_2 \phi(\xi) \left[1 + \sum_{j=1}^m v_j G_j(\xi) \right] \right) \\ &\quad \cdot \log \left(a_1 \phi(\xi) \left[1 + \sum_{j=1}^m u_j G_j(\xi) \right] \right. \\ &\quad \left. + a_2 \phi(\xi) \left[1 + \sum_{j=1}^m v_j G_j(\xi) \right] \right) d\xi \\ &= - \int_{\Xi} \phi(\xi) \left(1 + \sum_j (a_1 u_j + a_2 v_j) G_j(\xi) \right) \\ &\quad \cdot \log \phi(\xi) \left(1 + \sum_j (a_1 u_j + a_2 v_j) G_j(\xi) \right) d\xi \\ &\approx H(v) - \frac{1}{2} \sum_{j=1}^m (a_1 u_j + a_2 v_j)^2. \end{aligned} \quad (13)$$

This shows that the same first order entropy approximation holds for the sum of densities. Denoting measurements inside the contour as u_j , and those outside as v_j , for $j = 1, \dots, m$, and using the approximate entropy expressions (11), (13) in the energy functional Eq. (12), it may be approximated as

$$\begin{aligned} \widehat{JS}_{a,2} &= H(v) - \frac{1}{2} \sum_{j=1}^m (a_1 u_j + a_2 v_j)^2 \\ &\quad - a_1 \left(H(v) - \frac{1}{2} \sum_j u_j^2 \right) \\ &\quad - a_2 \left(H(v) - \frac{1}{2} \sum_j v_j^2 \right) \\ &= \frac{1}{2} \sum_{j=1}^m (-(a_1 u_j + a_2 v_j)^2 + a_1 u_j^2 + a_2 v_j^2) \\ &= \frac{1}{2} a_1 a_2 \sum_{j=1}^m (u_j - v_j)^2 \end{aligned} \quad (14)$$

by noting that $a_1 + a_2 = 1$.

Note that on account of the higher order nature of the coefficients u_j and v_j (i.e. higher order than first and second moments), the proposed energy functional subsumes the previously proposed techniques based

on the first and second order statistics. Those may in fact be shown to be particular cases of the above. This may also be justified by the fact that non-Gaussian densities may be expanded and that their higher order cumulants reflect the degree (or the lack thereof) of skewness or kurtosis of a density relative to a normal (Kendall and Stuart, 1958), hence $G(\xi) = \xi^3$, and $G(\xi) = \xi^4$, would be particular choices for the measurement functions G_j . Other choices of these functions; $G_1(\xi) = \xi e^{-\xi^2/2}$ as an odd function to measure asymmetry (analogous to the third moment as a measure of skewness), and $G_2(\xi) = |\xi|$, or $e^{-\xi^2/2}$ as choices of even functions (analogous to the fourth moment as a measure of sparsity, bimodality, relative to a Gaussian density), are given in Hyvarinen (1997) and Hyvarinen and Oja (2000). The idea behind using expectations of odd and even functions of the data is thus similar to attempts to characterize a density by the first few moments (usually the order is less than 4). The choice of priors a_i for each density is explained next:

- If we assign constant priors a_1 and a_2 (e.g. equal priors $a_1 = a_2 = 0.5$) for both of the regions, the constant $a_1 a_2 / 2$ multiplying the energy functional in Eq. (14) has no effect in terms of its first variation, and the gradient descent flow of the active contour that minimizes the energy functional $E = -\widehat{J}S_{a,2} = -\frac{1}{2}a_1 a_2 \sum_{j=1}^m (u_j - v_j)^2$ may be obtained by taking its first variation as

$$\frac{\partial \mathcal{C}}{\partial t} = \nabla \widehat{J}S_{a,2} = \sum_{j=1}^m (u_j - v_j)(\nabla u_j - \nabla v_j), \quad (15)$$

where a continuous active contour \mathcal{C} is utilized. As we have noted in the previous section, the resulting flow can be directly applied to an active polygon instead of a continuous active contour. A measurement or a constraint on a region distribution; u_j (resp. v_j) for region R_u (resp. R_v), is given by

$$\begin{aligned} u_j &= \frac{\int_{R_u} G_j(I(x, y)) dx dy}{|R_u|}, \\ v_j &= \frac{\int_{\Omega \setminus R_u} G_j(I(x, y)) dx dy}{|R_v|}. \end{aligned} \quad (16)$$

with $|R_u| = \int_{R_u} dx dy$, $|R_v| = \int_{\Omega \setminus R_u} dx dy$, and for $j = 1, \dots, m$ different constraints. Then the partial variation of u_j and v_j in Eq. (16) w.r.t \mathcal{C} is given

by

$$\begin{aligned} \nabla_{\mathcal{C}} u_j &= \frac{G_j(I) - u_j}{|R_u|} \mathbf{N}_u, \\ \nabla_{\mathcal{C}} v_j &= -\frac{G_j(I) - v_j}{|R_v|} \mathbf{N}_u, \end{aligned} \quad (17)$$

where \mathbf{N}_u denotes the outward unit normal of \mathcal{C} (region R_u). Note that the outward unit normal for the boundary of the outer region is $-\mathbf{N}_u$.

The contour evolution is found by substituting Eqs. (17) into the gradient descent flow Eq. (15):

$$\begin{aligned} \frac{\partial \mathcal{C}}{\partial t} &= f \mathbf{N}_u, \quad \text{where} \\ f &= \sum_{j=1}^m (u_j - v_j) \left(\frac{G_j(I(x, y)) - u_j}{|R_u|} \right. \\ &\quad \left. + \frac{G_j(I(x, y)) - v_j}{|R_v|} \right). \end{aligned} \quad (18)$$

We note that this is a generalized form of the data term of the flow proposed by Yezzi et al. (1999, 2002). In the above equation, the speed f of the contour along its normal direction, can be directly used in the active polygon evolution equation derived in Eq. (6), and restated in Eq. (7).

- On the other hand, in Eq. (14) we may assign variable weights a_1 , and a_2 that depend on the regions. An intuitive choice would be to pick the ratio of the area of each region to the total area of the image domain, say $A = |R_u| + |R_v|$. This choice in practice implies taking into account the number of pixels in each region, and would thus lead to a measure that is normalized with respect to the areas of the regions. Letting $a_1 = \frac{|R_u|}{A}$, $a_2 = \frac{|R_v|}{A}$, we then have to take into account in the derivation of the gradient descent flow, the first variations of the coefficient terms as well:

$$\begin{aligned} \frac{\partial \mathcal{C}}{\partial t} &= \nabla \widehat{J}S_{a,2} \\ &= \sum_{j=1}^m \frac{1}{2} \frac{|R_u| |R_v|}{A^2} (2(u_j - v_j)(\nabla u_j - \nabla v_j)) \mathbf{N}_u \\ &\quad + \frac{1}{2} \frac{|R_v|}{A^2} (u_j - v_j)^2 \mathbf{N}_u - \frac{1}{2} \frac{|R_u|}{A^2} (u_j - v_j)^2 \mathbf{N}_u. \end{aligned} \quad (19)$$

After some manipulations (given in Appendix B), this gradient descent flow can be written

as

$$\begin{aligned} \frac{\partial \mathcal{C}}{\partial t} &= f N_u, \quad \text{where} \\ f &= \frac{1}{2A} \sum_{j=1}^m (u_j - v_j) ((G_j(I) - u_j) \\ &\quad + (G_j(I) - v_j)) \end{aligned} \quad (20)$$

whose energy functional is indeed a generalized form of the external energy functional that Chan and Vese proposed in (1999):

$$\begin{aligned} E_{CV} &= \frac{1}{2A} \sum_{j=1}^m \int_{R_u} (G_j(I) - u_j)^2 dx dy \\ &\quad + \int_{R_v} (G_j(I) - v_j)^2 dx dy. \end{aligned} \quad (21)$$

We also note here that in the presence of severe noise, as illustrated in Fig. 1 for a uniform noise, the continuous contour ends up encircling small noisy regions, and its length grows. To overcome such effects, a penalty on the length of an active contour is added to its energy functional $E = \iint_R f dx dy + \alpha \oint_C ds$, where $\alpha \geq 0$, and s is the arclength of \mathcal{C} . This second term brings a problematic trade-off which we avoid in active polygon framework as will be explained next.

The advantage of propagating a polygon instead of a continuous curve, is demonstrated in Fig. 3, where a synthetic texture with vertical stripes is given. Obviously, thresholding for segmentation will not work since one of the stripes has the same color as the background. A continuous active contour propagation fails with a small regularization, i.e. small α mentioned in the previous paragraph, because the curve dips down into the gaps of the stripes with the same color as the background, and the individual bars are captured. With an increased amount of regularization (higher α) on



Figure 3. A continuous contour with a small regularization (first two), fails to capture as a whole an object with a synthetic texture of vertical stripes, whereas with a large regularization (middle two), rounds off the boundaries, and continues to shrink without sticking to the data. A polygonal contour (last two) correctly segments the textured region.

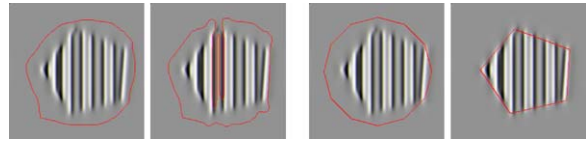


Figure 4. An active contour (first two) fails to capture synthetic texture of vertical stripes even after a Gabor filtering, whereas the active polygon (last two) captures the outline of the textured region.

the continuous curve (middle two images), the curve remains intact, however corners are rounded, and if one maintains the evolution, the important features will be “missed”. We have not been successful at obtaining the appropriate tradeoff between the data term and the regularizer in the continuous case to yield a satisfactory result. Active polygon propagation in Eq. (6) with f in (20) accurately and consistently captures the target shape. We also show in Fig. 4, the Gabor-filtered version of the same synthetic textured object, (tuned for vertical orientation). It, however, can be observed that the active contour still fails to operate on the filtered texture, whereas the active polygon again successfully captures the outline of the target region.

3.2. Evolution of Multiple Active Contours

A nice property of the Jensen-Shannon divergence measure is that it may be generalized as a probabilistic difference measure among any finite number of probability densities. Coupled propagation equations for multiple active contours which delineate different regions on an image domain can also be obtained as the gradient ascent flow of the JS divergence measure among the densities of those regions (note that we are trying to maximize the distance among the densities of regions). There is flexibility in the placement of the contours, which may delineate distinct or overlapping regions without difficulty. We again derive the gradient flows generally with respect to continuous contours. Figure 5 depicts two active contours whose inner regions are denoted by R_u , and R_v , and their common exterior by R_w . The measurements, i.e. statistics, in these respective regions are denoted by $u_j, v_j, w_j, j = 1, \dots, m$ for m different measurements, with respective prior probabilities $a_1, a_2, a_3 : a_1 + a_2 + a_3 = 1$. The energy functional for three

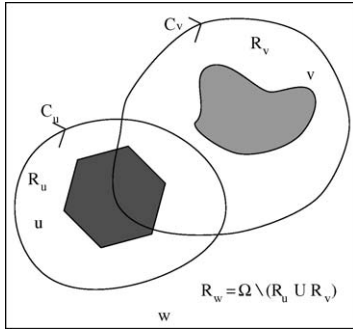


Figure 5. Ternary image regions.

densities can be written as

$$\begin{aligned}
 JS_{a,3} &= H\left(\sum_{i=1}^3 a_i p_i(\xi)\right) - \sum_{i=1}^3 a_i H(p_i(\xi)) \\
 &\approx H(v) - \frac{1}{2} \sum_{j=1}^m (a_1 u_j + a_2 v_j + a_3 w_j)^2 \\
 &\quad - a_1 \left(H(v) - \frac{1}{2} \sum_j u_j^2 \right) \\
 &\quad - a_2 \left(H(v) - \frac{1}{2} \sum_j v_j^2 \right) \\
 &\quad - a_3 \left(H(v) - \frac{1}{2} \sum_j w_j^2 \right) \\
 \widehat{JS}_{a,3} &= \frac{1}{2} \sum_{j=1}^m (a_1 a_2 (u_j - v_j)^2 + a_1 a_3 (u_j - w_j)^2 \\
 &\quad + a_2 a_3 (v_j - w_j)^2). \quad (22)
 \end{aligned}$$

This form of energy functional may easily be extrapolated to three active contours, thus four regions with statistics u_j, v_j, w_j, z_j ,

$$\begin{aligned}
 \widehat{JS}_{a,4} &= \frac{1}{2} \sum_{j=1}^m a_1 a_2 (u_j - v_j)^2 + a_1 a_3 (u_j - w_j)^2 \\
 &\quad + a_1 a_4 (u_j - z_j)^2 + a_2 a_3 (v_j - w_j)^2 \\
 &\quad + a_2 a_4 (v_j - z_j)^2 + a_3 a_4 (w_j - z_j)^2. \quad (23)
 \end{aligned}$$

The prior probabilities of each density a_1, \dots, a_4 may be selected in a variety of ways with the simplest selection being the equal priors, i.e. $a_i = 0.25$, $i = 1, \dots, 4$. It is now straightforward to approximate the JS functional $\widehat{JS}_{a,N}$ for N regions

on the image domain. It may be observed that the first-order approximations to both the densities and the corresponding entropies of the regions, lead to an overall measure that computes a weighted sum of the divergence measures (i.e. distances between their statistics) between all pairwise combinations of the regions.

Active contour evolutions for three regions using means and variances as statistics of each region were derived from a totally different perspective by Yezzi et al. (1999). Their energy functional was based on a geometric notion which maximized the area of a triangle formed by the statistics of the three regions. Our energy functional on the other hand, is information-theoretic in nature, and evaluates the distance among probability densities.

The ternary case entails the derivation of a gradient flow for each of the two active contours C_u , and C_v . Taking the first variation of the energy functional in Eq. (22) w.r.t. the contour C_u , yields

$$\begin{aligned}
 \nabla_{\mathbf{c}_u} \widehat{JS}_{a,3} &= \sum_{j=1}^m [a_1 a_2 (u_j - v_j) + a_1 a_3 (u_j - w_j)] \\
 &\quad \times \nabla_{\mathbf{c}_u} u_j - [a_1 a_3 (u_j - w_j) \\
 &\quad + a_2 a_3 (v_j - w_j)] \nabla_{\mathbf{c}_u} w_j \quad (24)
 \end{aligned}$$

where we used the fact that $\nabla_{\mathbf{c}_u} v_j = 0$, $\forall j$, since v_j are the statistics inside the contour C_v which do not depend on the contour C_u .

The partial variation of w_j 's requires more attention than that of u_j 's and v_j 's since the statistic w_j is calculated over the common exterior of both contours whose boundary may not be smooth when the two contours overlap. We exploit a similar strategy given in Yezzi et al. (1999) to express a statistic in this third region using characteristic functions χ_u, χ_v over the regions R_u, R_v as

$$w_j = \frac{\int_{\Omega \setminus R_u} G_j(I) (1 - \chi_v) dx dy}{\int_{\Omega \setminus R_u} (1 - \chi_v) dx dy}$$

where the denominator may be renamed as $|R_w|$. The variation of w_j w.r.t. C_u can hence be obtained as

$$\nabla_{\mathbf{c}_u} w_j = -\frac{G_j(I) - w_j}{|R_w|} (1 - \chi_v) \mathbf{N}_u. \quad (25)$$

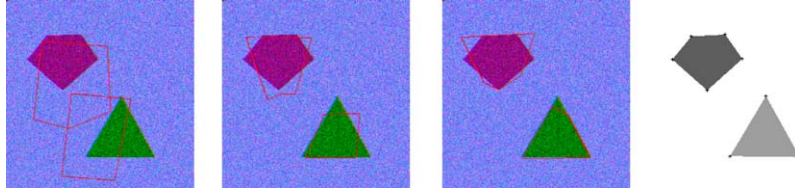


Figure 6. Ternary flows using image forces with $G(x) = x$, are used to segment this simple ternary image corrupted by Gaussian noise. Output of the algorithm shown on the right provides only 5 vertex locations for the first object, and 3 vertex locations for the second object.

The gradient descent flow of the contour C_u which is equal to $\nabla_{\mathbf{c}_u} \widehat{J}S_{a,3}$ is thus obtained as $\frac{\partial \mathbf{C}_u}{\partial t} = f_u \mathbf{N}_u$, where

$$f_u = \sum_{j=1}^m [a_1 a_2 (u_j - v_j) + a_1 a_3 (u_j - w_j)] \times \frac{G_j(I(x, y)) - u_j}{|R_u|} + [a_1 a_3 (u_j - w_j) + a_2 a_3 (v_j - w_j)] \frac{G_j(I(x, y)) - w_j}{|R_w|} (1 - \chi_v). \quad (26)$$

By similar arguments, one can write $w_j = \frac{\int_{\Omega \setminus R_v} G_j(I) (1 - \chi_u) dx dy}{\int_{\Omega \setminus R_v} (1 - \chi_u) dx dy}$, where the denominator is equal to $|R_w|$, the variation of w_j w.r.t C_v can be obtained as

$$\nabla_{\mathbf{c}_v} w_j = - \frac{G_j(I) - w_j}{|R_w|} (1 - \chi_u) \mathbf{N}_v. \quad (27)$$

Then taking the first variation of the energy functional in Eq. (22) w.r.t. the contour C_v , and noting that $\nabla_{\mathbf{c}_v} u_j = 0$, $\forall j$, leads to the gradient flow of the contour C_v , $\frac{\partial \mathbf{C}_v}{\partial t} = f_v \mathbf{N}_v$, where

$$f_v = \sum_{j=1}^m [-a_1 a_2 (u_j - v_j) + a_2 a_3 (v_j - w_j)] \times \frac{G_j(I(x, y)) - v_j}{|R_v|} + [a_1 a_3 (u_j - w_j) + a_2 a_3 (v_j - w_j)] \frac{G_j(I(x, y)) - w_j}{|R_w|} (1 - \chi_u). \quad (28)$$

The two speed functions f_u and f_v when inserted into Eq. (6) for two separate polygon propagations, C_u and C_v , result in ternary polygonal flows.

We illustrate in Fig. 6, the ternary case for polygon propagations with f_u and f_v given in Eq. (26) and Eq. (28). Although, the polygonal contours C_u and C_v evolve separately, their motion is coupled through the variables in the evolution equations that depend on each of the three regions. Two contours move in such a way to maximize the approximate Jensen-Shannon divergence among densities of the three regions, namely R_u : inside the contour C_u ; R_v : inside the contour C_v ; R_w : the complement of $R_u \cup R_v$. Only means are used as the separating statistics, (i.e., $j = 1$, $G(x) = x$), and the resulting two polygons are shown in Fig. 6 (right). Hence, the gain is again two-fold: segmentation of the targets, and their description in terms of a handful of vertices are both achieved.

4. A Global Polygon Regularizer

The flow of an active polygon may, under the sole influence of a data term, become undefined (degenerate) under a variety of scenarios, e.g. when a vertex becomes infinitesimally close to a non-neighbor edge of the polygon, or when two vertices or two edges come infinitesimally close to each other at some point. We show such an example in Fig. 7, in which propagation of an initial polygon with 5 vertices becomes degenerate, where the vertex V_4 approaches (then crosses) the edge between vertices V_2 and V_3 . As a solution to overcome this problem, we introduce a natural regularizing term well adapted to an evolving polygon, which would not be computationally feasible for smooth continuous contours. This regularization is accomplished by first viewing each edge of the polygon as a finite line charge of uniform charge density. We compute an electric field \mathbf{E} , generated by a finite uniform line charge (\mathbf{a}, \mathbf{b}) (depicted in Fig. 8), exerted on a point charge, and the total electric field $\mathbf{E}_{ab}(\mathbf{x}')$ can be written in terms of the two-vectors $\mathbf{x}_a = \mathbf{x}' - \mathbf{a}$ and

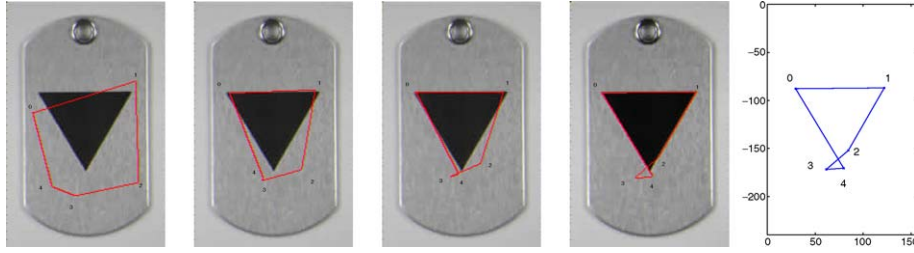


Figure 7. We demonstrate that flow (6) may become degenerate without an additional constraint on the motion of vertices.

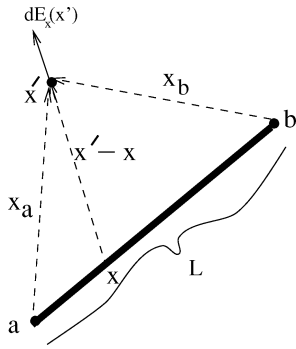


Figure 8. Calculation of the electric force exerted by a line charge (a, b) at a point x' on the polygon.

$$\mathbf{x}_b = \mathbf{x}' - \mathbf{b},$$

$$\begin{aligned} \mathbf{E}_{ab}(\mathbf{x}') &= \frac{k_c L}{\|\mathbf{x}_a\|^2 \|\mathbf{x}_b\|^2 - (\mathbf{x}_a \cdot \mathbf{x}_b)^2} \\ &\times \left(\frac{\|\mathbf{x}_b\|^2 \mathbf{x}_a - (\mathbf{x}_a \cdot \mathbf{x}_b) \mathbf{x}_b}{\|\mathbf{x}_b\|} \right. \\ &\left. + \frac{\|\mathbf{x}_a\|^2 \mathbf{x}_b - (\mathbf{x}_a \cdot \mathbf{x}_b) \mathbf{x}_a}{\|\mathbf{x}_a\|} \right). \end{aligned} \quad (29)$$

For details of this derivations, we refer to Appendix C.

As shown in the previous section, a data term corresponding to a given vertex consists of an integrated force along its two neighboring edges. In a similar way, an electric field exerted at a vertex is also integrated along two neighboring edges. Evolution of a polygon vertex \mathbf{V}_k , due to the total electric field \mathbf{E}_k integrated along two neighbor edges ($\mathbf{V}_{k-1}, \mathbf{V}_k$) and ($\mathbf{V}_k, \mathbf{V}_{k+1}$) may then be written as

$$\begin{aligned} \frac{\partial \mathbf{V}_k}{\partial t} = \mathbf{E}_k &= \sum_{\substack{j=0 \\ j \neq k, j \neq k-1}}^n \int_0^1 p \mathbf{E}_{\mathbf{V}_{j-1}, \mathbf{V}_j} \\ &\times (p \mathbf{V}_k + (1-p) \mathbf{V}_{k-1}) dp \end{aligned}$$

$$\begin{aligned} &+ \sum_{\substack{j=0 \\ j \neq k, j \neq k+1}}^n \int_0^1 (1-p) \mathbf{E}_{\mathbf{V}_j, \mathbf{V}_{j+1}} \\ &\times ((1-p) \mathbf{V}_k + p \mathbf{V}_{k+1}) dp. \end{aligned} \quad (30)$$

This global, rather than local, geometric dependence makes this regularizer very different from the ones used in the literature. The use of a global regularizer is more consistent with the desire to capture local features that would otherwise not be captured. Thus, the additional and novel geometric component of the polygon evolver, which induces global geometric dependence, provides a regularization which both avoids the flow degeneracy as well as captures sharp corners of the target shape without any shrinking or smoothing effects.

We demonstrate the polygon regularization capability of the electric force flow in Eq. (30) in Fig. 9 for two different polygons. The polygonal evolution with an electrostatic regularizer force (plotted at each vertex) is shown at several snapshots in these figures. Note how the force at each vertex is large in magnitude initially, and push a vertex away from the other edges of the polygon. The magnitude of the electric force at each vertex decreases and edges

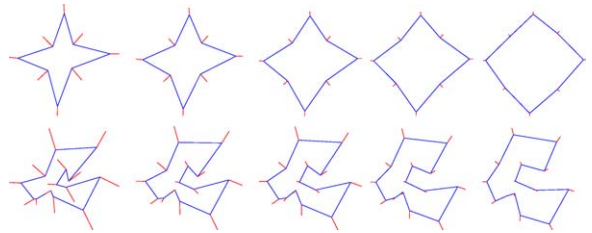


Figure 9. Electrostatic regularizer in Eq. (30) computes the electric force at each vertex.

remain well apart which is exactly the effect we expect from the regularizer force. This force should be insignificant when a vertex and its adjacent edges are not very close to most of the other edges, and should become influential, even dominate when the vertex or its adjacent edges are very close to other edges.

The addition of the regularizer term (30) to the motion equation of a vertex obtained in Eq. (6) leads to the following modified vertex flow

$$\frac{\partial \mathbf{V}_k}{\partial t} = \alpha \left\{ \int_0^1 pf(L(p, \mathbf{V}_{k-1}, \mathbf{V}_k)) dp \mathbf{N}_{k,k-1} + \int_0^1 (1-p)f(L(p, \mathbf{V}_k, \mathbf{V}_{k+1})) dp \mathbf{N}_{k+1,k} \right\} + (1-\alpha)\mathbf{E}_k. \quad (31)$$

Here, α , a constant parameter to weight the influence of data term, and the electric field term, is chosen as 0.95 throughout the evolutions. The reason that we put such a heavy weight on the data term is that the regularizer only kicks in very powerfully when degeneracy occurs, and it lets the data term govern the evolution of the polygon during most of the evolution time.

In Fig. 10 we demonstrate the use of flow (31) for the same initial active polygon with 5 vertices which has been shown to result in an ill-posed flow in the previous section in Fig. 7. Here, snapshots of only the active polygon on the triangle shape image are given to better appreciate the influence of the regularizer, and we show the electric force at each vertex during this evolution. Note that the electric force at a vertex becomes significantly large when the vertex is infinitesimally close to another edge in this figure. This event exactly keeps the polygon simple during the evolution,

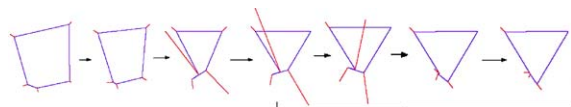


Figure 10. The electric forces for an evolution are shown. Note the forces only become significant when a vertex approaches another vertex or edge.

and by the effect of the data term, the polygon converges to the target shape.

5. Results and Conclusions

In this paper, we have presented a new approach for image segmentation through polygon propagating equations. In this section, by way of numerical experiments, we validate the effectiveness and the usefulness of our technique.

5.1. Implementation Issues

The performance of most active contour algorithms depend on the initial conditions (Zhu and Yuille, 1996). A particularly important question in carrying out such flows, is that of initializing the contour. Specifically in our case, we need to specify the number of vertices, and their placement to start off the evolution of the polygon. For the active polygons, though, it is possible to circumvent this problem, and speed up the convergence, by a simple approach which helps an initial active polygon adaptively adjust to the number of vertices required for the description of the target shape. Towards that end, we may initialize a very coarse polygon with a small number of vertices, e.g. a big rectangular or circular polygon close to the image boundaries. While the initial polygon, usually with very few vertices, is propagating with both the image force and the regularizer force, new vertices are periodically added and removed affording it a flexible motion towards the target region. A natural criterion to remove a vertex may for instance be based on the angle between its two adjacent edges being close to either 0, or π . This may be effected for a given vertex \mathbf{V}_k , with its adjacent edges $\mathbf{A} = (\mathbf{V}_{k-1} - \mathbf{V}_k)$, and $\mathbf{B} = (\mathbf{V}_{k+1} - \mathbf{V}_k)$, by computing the following inner product $\mathbf{A} \cdot \mathbf{B} = \|\mathbf{A}\| \|\mathbf{B}\| \cos(\theta_{AB})$, the θ_{AB} being the angle between the two vectors. One may therefore check if

$$|\cos(\theta_{AB})| = \frac{|\mathbf{A} \cdot \mathbf{B}|}{\|\mathbf{A}\| \|\mathbf{B}\|} \approx 1, \quad (32)$$

to determine the redundancy of a vertex. In either case, the vertex \mathbf{V}_k may simply be removed from the vertex list, to finally yield a polygon properly enclosing the shape. During a vertex addition period of an evolution, the magnitude of our image force along each edge

of a polygon, i.e. $D = \int_0^1 |f(L(p, \mathbf{V}_k, \mathbf{V}_{k+1}))| dp$, is computed, and a new vertex is added to a middle point of the edge with the maximum value of D . The intuition here is that the edges with higher image speeds are closer to image structures that may require finer details.

For implementational purposes, the polygon structure P is a two-vector (2-D vector), and the normals needed in the computation of Eq. (31) are computed as $\mathbf{N}_{k,k-1} = (-P(k, 1) + P(k-1, 1), P(k, 0) - P(k-1, 0))^T$. We also maintain a two-dimensional function which acts as an indicator function to show which pixel is inside or outside a polygon during the evolution to facilitate computation of the statistics in the regions. Statistical calculations may be carried out fast by computing the change in the position of each polygon edge, and appropriately adding or subtracting the statistics computed in that difference region, which results in the motion of the edge, which is a straight line, from one iteration to the next. Time step in the discretization of the ODE is chosen large, e.g. $\delta t = 10$, which indeed helps the model to escape various local minima of the objective function. For a typical image of roughly 250×300 size, the relative speed of the active polygon model is approximately twice that of an associated active contour model using the same data term, and runs on the order of a few seconds.

As we mentioned, we may also add a random perturbation to our ODE model, a zero-mean Gaussian

r.v. with a variance that has a very minor effect when compared to the change in the image term. This trivial perturbation changes the path of each evolution very slightly although the results are very consistent as will be shown next.

5.2. Experimental Results

In this section, we demonstrate texture segmentation examples on natural texture images. Our active polygon propagation model is in Eq. (31) with speed function in (20), and measurement functions $G_1(\xi) = \xi e^{-\xi^2/2}$, $G_2(\xi) = e^{-\xi^2/2}$, $G_3 = |\xi|$, $G_4 = \log(\cosh(x))$.

In the first example, a zebra on a grassy background constitutes of mainly two textured regions (Fig. 11). A generic rectangle, i.e. just four vertices, is initialized on the zebra image which is quite challenging in terms of unsupervised texture segmentation. Snapshots from the polygon propagation with the resulting segmentation in Fig. 11, show that a zebra figure is very nicely captured.

Other natural texture examples include a monarch larvae and a monarch butterfly with generic polygon initializations, a circle and a rectangle, are shown in Fig. 12. In the same figure, another arbitrary initialization on the same monarch picture, show that the target textured body of the monarch is captured in both cases.

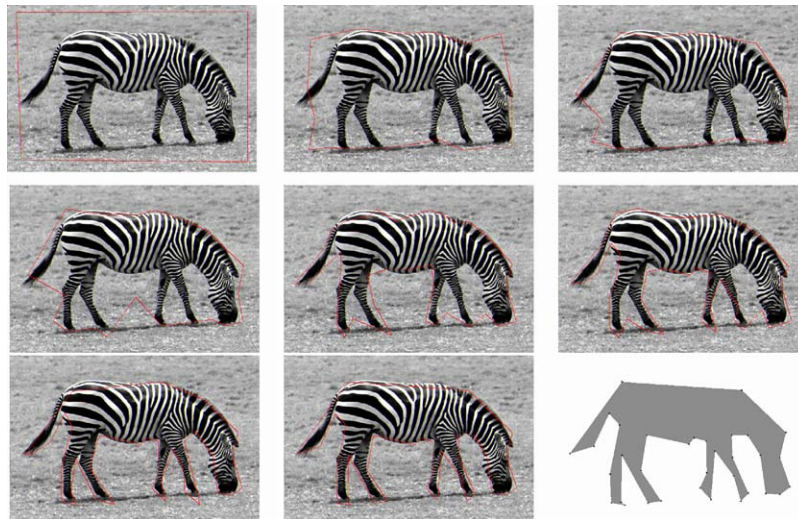


Figure 11. A zebra figure is captured by the active polygon model. A generic rectangular active polygon close to image boundaries is initialized.

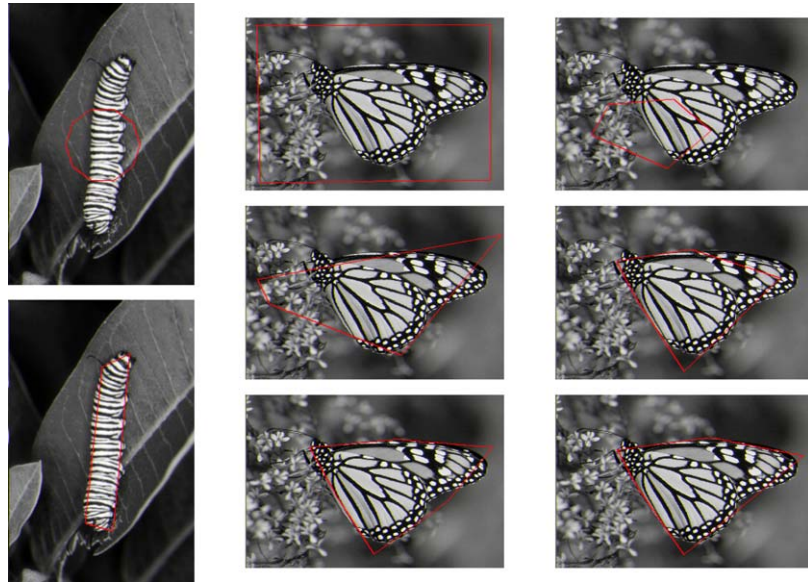


Figure 12. A monarch larvae on a leaf is captured by an active polygon (left). Monarch butterfly is captured in the two other columns with very different initializations.

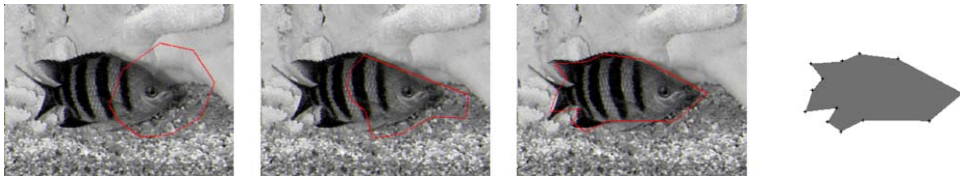


Figure 13. A fish with a striped texture is captured.

In Fig. 13, a fish whose body has a texture of stripes is captured by an active polygon. Similarly, a sea star on a textured rocky terrain, (Fig. 14), a cheetah figure (Fig. 15 left), another cheetah in bushes (Fig. 15

right), and a chunk of crystal (Fig. 16) are shown to demonstrate texture capturing capabilities of the active polygon model together with the Jensen-Shannon criterion.

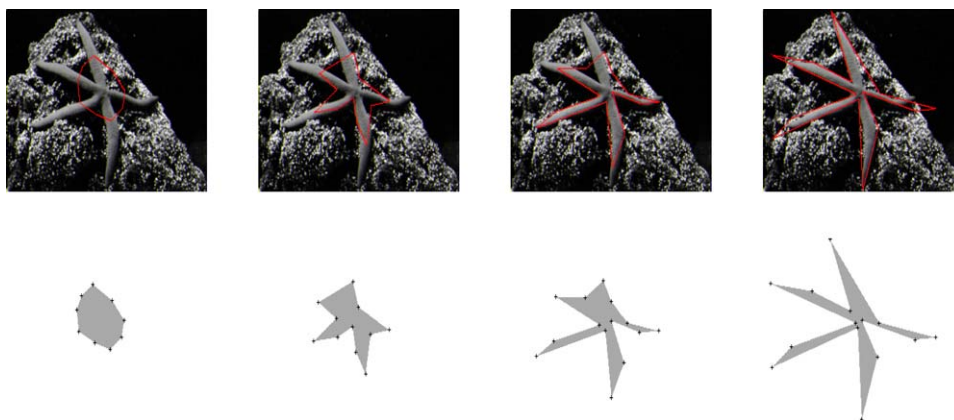


Figure 14. A sea star embedded in a textured rocky background is captured.

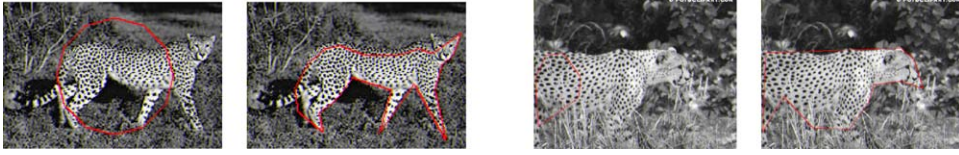


Figure 15. Cheetah figures are captured by active polygons.

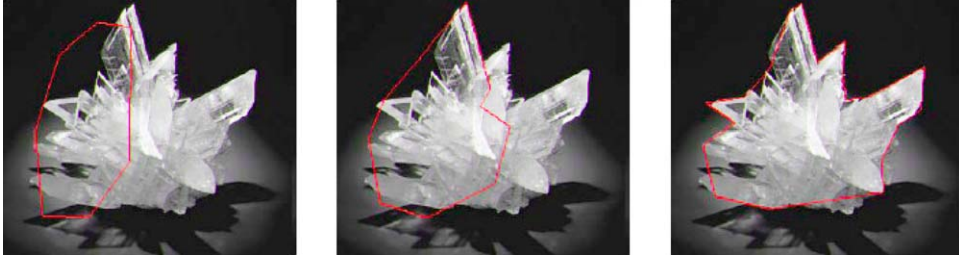


Figure 16. A natural crystal chunk is captured.

One of our goals was to apply our active polygon model to capture man-made object shapes. A group of real airplane image experiments on each of which a generic circular polygon was initialized, are shown in Fig. 17. Our model successfully captures the plane shape in terms of a polygon, which may be essential as an input to object recognition algorithms. An image of another man-made object, a submarine, is shown in Fig. 18.

Our active polygon technique is also suitable for document image segmentation because a document page usually has two different kinds of texture, namely text and images, which have distinct probability distributions. We show two examples of document segmentation: Fig. 19 with a single active polygon, and Fig. 20 with two active polygons.

5.3. Conclusions and Future Work

In this paper, we have presented a polygon propagation model to capture particularly textured objects in images. A new ODE model was developed to move polygon vertices. In addition, a new global polygon regularizer was introduced to avoid degeneracy during polygon propagation. Adaptation of a favorable divergence measure, the Jensen-Shannon divergence, as an integral form (energy functional) of our ODEs lead to quite a powerful unsupervised texture segmentation technique which was validated by numerical results. The only assumption, which is valid in

many applications, in our model on the target image regions is, that they should be simply connected. This is on account of most of the cases, whether in natural images as in zebra, or man-made object images as in airplanes, texture regions are simply connected.

Future Work. Many real applications tailored to the representation provided by our model are currently under investigation. An object tracking application may take advantage of a polygonal representation, and together with an optical flow estimation in an active polygon spirit are reported in Unal et al. (2002). Another application we are working on, is in object recognition, where a description of shapes or objects with a handful of vertices would be essential for object-based description and recognition tasks, particularly along the same context of the very recent MPEG-7 standard.

Appendix A: Derivation of ODEs for Vertex Motion

Let us define C_v for vertex V_i by

$$C_v(p, V) = \begin{cases} (p - (i - 1))\mathbf{e} & \text{for } i - 1 \leq p \leq i \\ (1 - (p - i))\mathbf{e} & \text{for } i \leq p \leq i + 1 \\ 0 & \text{for } |p - i| \geq 2 \end{cases}$$

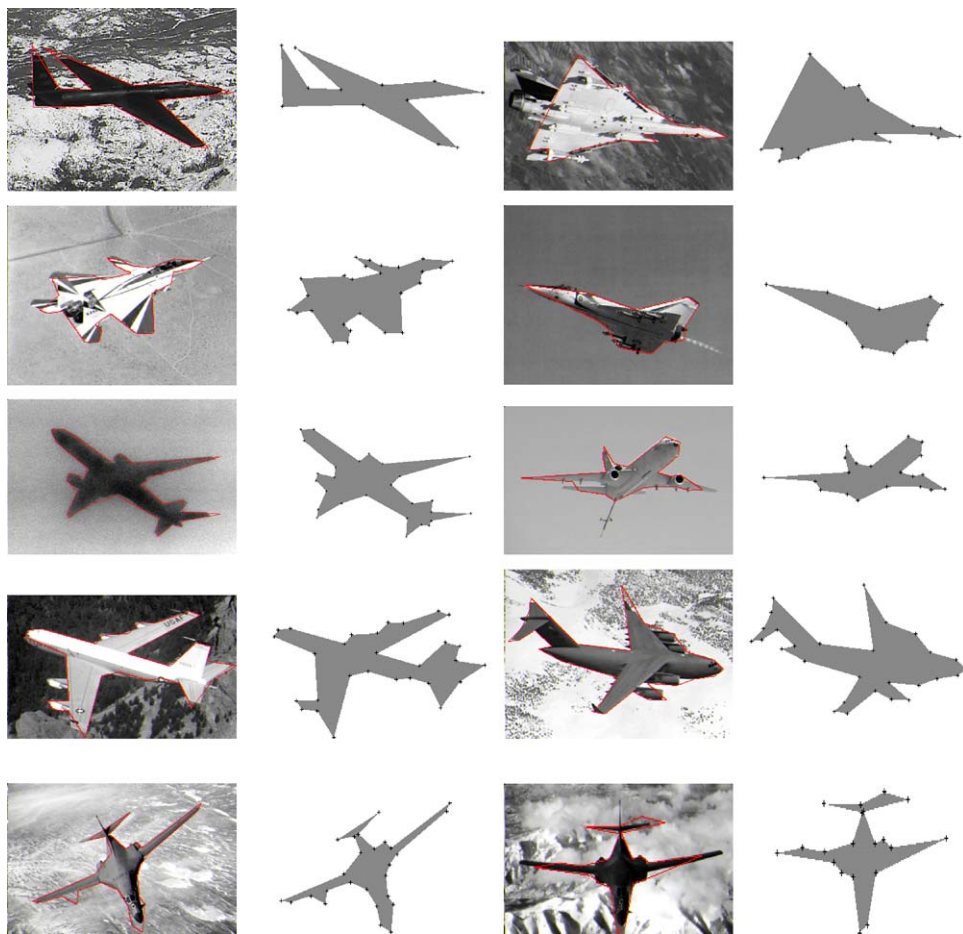


Figure 17. Each airplane is captured by a handful of vertices.

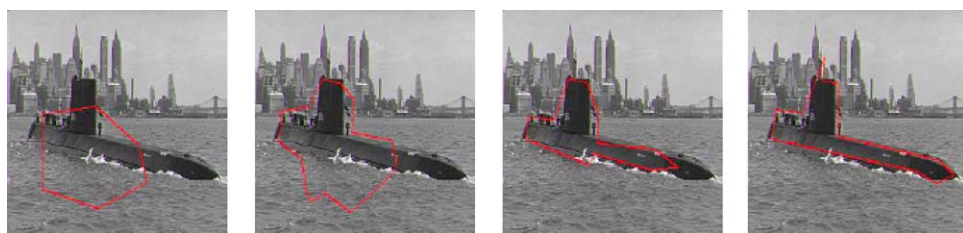


Figure 18. A submarine figure is captured by a handful of vertices.

where $\mathbf{e} \in \{\mathbf{e}_x, \mathbf{e}_y\}$ denote the standard bases for \mathbb{R}^2 . We now write our energy as a function of the vertices $\mathbf{V} : E(\mathbf{V}) = \int_0^n \langle \mathbf{F}, \mathbf{N} \rangle \| \mathbf{C}_p \| dp = \int_0^n \langle \mathbf{F}, \mathbf{J}\mathbf{C}_p \rangle dp$, and compute its partial derivative with respect to one of the vertex coordinates v where either $v = x_i$ or $v = y_i$ for some $1 \leq i \leq n$, as $E_v(\mathbf{V}) = \int_0^n f \langle \mathbf{C}_v, \mathbf{J}\mathbf{C}_p \rangle dp$. Substituting the particular forms

of \mathbf{C} , \mathbf{C}_p (Eq. (4)), and \mathbf{C}_v (the latter denoting either \mathbf{C}_{x_i} or \mathbf{C}_{y_i} for some vertex i) into this expression yields

$$E_v = \int_0^n f(L(p - \lfloor p \rfloor, \mathbf{V}_{\lfloor p \rfloor}, \mathbf{V}_{\lfloor p \rfloor + 1})) \times \langle \mathbf{C}_v, \mathbf{J}(\mathbf{V}_{\lfloor p \rfloor + 1} - \mathbf{V}_{\lfloor p \rfloor}) \rangle dp$$

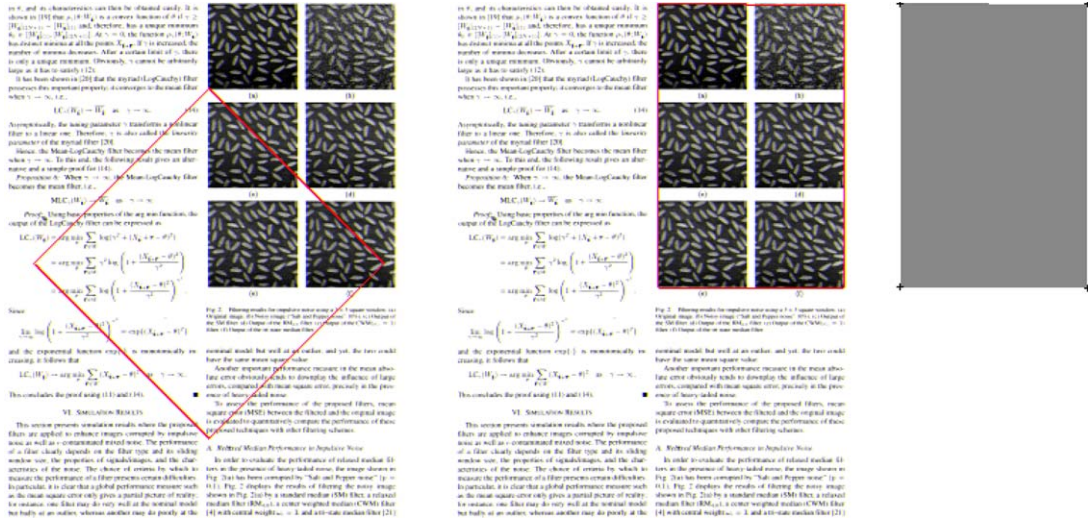


Figure 19. An active polygon nicely segments a document image scanned from an article.



Figure 20. Two active polygons capture text and image regions of a page from an article.

$$\begin{aligned}
 &= \sum_{k=0}^{n-1} \int_0^1 f(L(p, \mathbf{V}_k, \mathbf{V}_{k+1})) \\
 &\quad \times \langle \mathbf{C}_v(p+k), J(\mathbf{V}_{k+1} - \mathbf{V}_k) \rangle dp \\
 &= \int_0^1 f(L(p, \mathbf{V}_{i-1}, \mathbf{V}_i)) \\
 &\quad \times \langle \mathbf{C}_v(p+i-1), J(\mathbf{V}_i - \mathbf{V}_{i-1}) \rangle dp \\
 &\quad + \int_0^1 f(L(p, \mathbf{V}_i, \mathbf{V}_{i+1})) \\
 &\quad \times \langle \mathbf{C}_v(p+i), J(\mathbf{V}_{i+1} - \mathbf{V}_i) \rangle dp \\
 &= \langle \mathbf{e}, J(\mathbf{V}_i - \mathbf{V}_{i-1}) \rangle \int_0^1 pf(L(p, \mathbf{V}_{i-1}, \mathbf{V}_i)) dp \\
 &\quad + \langle \mathbf{e}, J(\mathbf{V}_{i+1} - \mathbf{V}_i) \rangle \\
 &\quad \times \int_0^1 (1-p)f(L(p, \mathbf{V}_i, \mathbf{V}_{i+1})) dp
 \end{aligned}$$

where $\mathbf{e} = \mathbf{e}_x$ if $v = x_i$ or $\mathbf{e} = \mathbf{e}_y$ if $v = y_i$. If we introduce a time variable t and evolve both coordinates x_i and y_i in the gradient directions given above, and denoting the corresponding $J(\mathbf{V}_i - \mathbf{V}_{i-1}) = N_{i,i-1}$, we obtain the following gradient flow for the vertex \mathbf{V}_i

$$\frac{\partial \mathbf{V}_i}{\partial t} = \int_0^1 pf(L(p, \mathbf{V}_{i-1}, \mathbf{V}_i)) dp N_{i,i-1} + \int_0^1 (1-p)f(L(p, \mathbf{V}_i, \mathbf{V}_{i+1})) dp N_{i+1,i}.$$

Appendix B: Derivation of the Gradient Flow for Varying Priors Proportional to the Areas

Rewriting here Eq. (19), (note that $A = |R_u| + |R_v|$),

$$\begin{aligned} \frac{\partial C}{\partial t} &= \nabla \widehat{J} S_{a,2} \\ &= \sum_{j=1}^m \frac{1}{2} \frac{|R_u||R_v|}{A^2} (2(u_j - v_j)(\nabla u_j - \nabla v_j)) N_u \\ &\quad + \frac{1}{2} \frac{|R_v|}{A^2} (u_j - v_j)^2 N_u - \frac{1}{2} \frac{|R_u|}{A^2} (u_j - v_j)^2 N_u, \end{aligned} \quad (33)$$

it may be rewritten as follows:

$$\begin{aligned} \frac{\partial C}{\partial t} &= \frac{N_u}{2A^2} \sum_{j=1}^m (u_j - v_j) g \left(\frac{2|R_u||R_v|(G_j(I) - u_j)}{|R_u|} \right. \\ &\quad \left. + \frac{2|R_u||R_v|(G_j(I) - v_j)}{|R_v|} \right. \\ &\quad \left. + (|R_v| - |R_u|)(u_j - v_j) \right) \\ &= \frac{N_u}{2A^2} \sum_{j=1}^m (u_j - v_j) (2|R_v|(G_j(I) - u_j) \\ &\quad + 2|R_u|(G_j(I) - v_j) + (|R_v| - |R_u|)(u_j - v_j)) \\ &= \frac{N_u}{2A^2} \sum_{j=1}^m (u_j - v_j) (2|R_v|G_j(I) - 2|R_v|u_j \\ &\quad + 2|R_u|G_j(I) - 2|R_u|v_j \\ &\quad + (|R_v| - |R_u|)(u_j - v_j)) \\ &= \frac{N_u}{2A^2} \sum_{j=1}^m (u_j - v_j) (2(|R_u| + |R_v|)G_j(I) \\ &\quad - |R_v|u_j - |R_u|v_j - |R_u|u_j - |R_v|v_j) \\ &= \frac{N_u}{2A} \sum_{j=1}^m (u_j - v_j) (G_j(I) - u_j + G_j(I) - v_j) \\ &= \frac{N_u}{2A} \sum_{j=1}^m [-(G_j(I) - u_j)^2 + (G_j(I) - v_j)^2]. \end{aligned} \quad (34)$$

It can be observed that Eq. (34) is the gradient descent flow for the following energy functional

$$\begin{aligned} E &= \frac{1}{2A} \sum_{j=1}^m \int_{R_u} (G_j(I) - u_j)^2 dx dy \\ &\quad + \int_{R_v} (G_j(I) - v_j)^2 dx dy, \end{aligned} \quad (35)$$

which is a generalized form of the energy functional proposed by Chan and Vese (1999).

Appendix C: Electric Force by a Line Charge

Given a line charge or a rod of positive charge that extends from a generic point $\mathbf{a} \in \mathbb{R}^3$ to $\mathbf{b} \in \mathbb{R}^3$, our goal is to calculate the electric field at a point $\mathbf{x}' \in \mathbb{R}^3$. Points are chosen in \mathbb{R}^3 , and using electrostatics principles, we consequently derive these fields for them. The line charge is assumed to be made up of differential point charges dq . We need to compute the differential electric field $d\mathbf{E}(\mathbf{x}')$ exerted at \mathbf{x}' by a charge dq at location $\mathbf{x} = \mathbf{a} + t(\mathbf{b} - \mathbf{a})$ which is on the rod (depicted in Fig. 8). As given by Coulomb's law (Ulaby, 1997), $d\mathbf{E}(\mathbf{x}')$ is inversely proportional to the square of the Euclidean distance $\|\mathbf{x}' - \mathbf{x}\|^2$ between \mathbf{x} and \mathbf{x}' , and its direction is given by the vector $(\mathbf{x}' - \mathbf{x})/\|\mathbf{x}' - \mathbf{x}\|$, i.e., $d\mathbf{E}(\mathbf{x}') = (\mathbf{x}' - \mathbf{x})/\|\mathbf{x}' - \mathbf{x}\|^3 dq$. We assume a uniform charge density λ (a constant parameter) along the rod, hence $dq = \lambda dx$. With the change of variable $\mathbf{x} = \mathbf{a} + t(\mathbf{b} - \mathbf{a})$, the differential amount of increase in $dx = L dt$, where $L = \|\mathbf{b} - \mathbf{a}\|$ is the length of the rod extending from \mathbf{a} to \mathbf{b} .

By the principle of superposition, the total electric field \mathbf{E} acting on point charge at \mathbf{x}' due to line charge (\mathbf{a}, \mathbf{b}) , can be obtained by integrating the fields contributed by all differential point charges on the rod making up the linear charge distribution,

$$\begin{aligned} \mathbf{E}_{ab}(\mathbf{x}') &= \int_{\mathbf{a}}^{\mathbf{b}} \frac{\mathbf{x}' - \mathbf{x}}{\|\mathbf{x}' - \mathbf{x}\|^3} \lambda dx \\ &= k_c L \int_0^1 \frac{(\mathbf{x}' - \mathbf{a}) + t(\mathbf{a} - \mathbf{b})}{\|(\mathbf{x}' - \mathbf{a}) + t(\mathbf{a} - \mathbf{b})\|^3} dt. \end{aligned} \quad (36)$$

Note that the constant λ is combined with the Coulomb's constant into a constant parameter called k_c . After some manipulations, the total electric field $\mathbf{E}_{ab}(\mathbf{x}')$ can be written in terms of the two-vectors $\mathbf{x}_a = \mathbf{x}' - \mathbf{a}$ and $\mathbf{x}_b = \mathbf{x}' - \mathbf{b}$ (depicted in Fig. 8),

$$\begin{aligned} \mathbf{E}_{ab}(\mathbf{x}') &= \frac{k_c L}{\|\mathbf{x}_a\|^2 \|\mathbf{x}_b\|^2 - (\mathbf{x}_a \cdot \mathbf{x}_b)^2} \\ &\quad \times \left(\frac{\|\mathbf{x}_b\|^2 \mathbf{x}_a - (\mathbf{x}_a \cdot \mathbf{x}_b) \mathbf{x}_b}{\|\mathbf{x}_b\|} \right. \\ &\quad \left. + \frac{\|\mathbf{x}_a\|^2 \mathbf{x}_b - (\mathbf{x}_a \cdot \mathbf{x}_b) \mathbf{x}_a}{\|\mathbf{x}_a\|} \right). \end{aligned} \quad (37)$$

References

- Besag, J. 1973. Spatial interaction and the statistical analysis of lattice systems. *J. Royal Stat. Soc. B*, 36:192–236.
- Blake, A. and Isard, M. 1998. *Active Contours*. Springer Verlag: London, Great Britain.
- Blake, A. and Zisserman, A. 1987. *Visual Reconstruction*. MIT Press: Cambridge, MA.
- Bruckstein, A., Sapiro, G., and Shaked, D. 1995. Evolutions of planar polygons. *Int. J. Pattern Recognition and Artificial Intell.*, 9(6):991–1014.
- Caselles, V., Catta, F., Coll, T., and Dibos, F. 1993. A geometric model for active contours in image processing. *Numerische Mathematik*, 66:1–31.
- Caselles, V., Kimmel, R., and Sapiro, G. 1995. Geodesic active contours. In *ICCV95*, pp. 694–699.
- Chakraborty, A., Staib, L., and Duncan, J. 1996. Deformable boundary finding in medical images by integrating gradient and region information. *IEEE Trans. on Medical Imaging*, 15(6):859–870.
- Chan, T.F. and Vese, L.A. 1999. An active contour model without edges. In *Int. Conf. Scale-Space Theories in Computer Vision*, pp. 141–151.
- Chan, T. and Vese, L. 2001. A level set algorithm for minimizing the Mumford-Shah functional in image processing. In *Proc. IEEE Workshop on Variational and Level Set Methods*.
- Chesnaud, C., Refregier, P., and Boulet, V. 1999. Statistical region snake-based segmentation adapted to different physical noise models. *PAMI*, 21:1145–1156.
- Cover, T.M. and Thomas, J.A. 1991. *Elements of Information Theory*. Wiley: New York.
- Cremers, D., Tischhäuser, F., Weickert, J., and Schnörr, C. 2002. Diffusion snakes: Introducing statistical shape knowledge into the Mumford-Shah functional. *Int. J. Computer Vision*, 50(3):295–313.
- Cross, G. and Jain, A.K. 1983. Markov random field texture models. *IEEE Trans. Pattern Analysis, and Machine Intelligence*, 5:25–39.
- Dunham, J.G. 1986. Optimum uniform piecewise linear approximation of planar curves. *IEEE Trans. Pattern Analysis, and Machine Intelligence*, 8:67–75.
- Figueiredo, M.A.T., Leitao, J.M.N., and Jain, A.K. 2000. Unsupervised contour representation and estimation using b-splines and a minimum description length criterion. *IEEE Trans. Image Process.*, 9(6):1075–1087.
- Freeman, H. 1978. Shape description via the use of critical points. *Pattern Recognition*, 10:159–166.
- Geman, S. and Geman, D. 1984. Stochastic relaxation, gibbs distribution, and the bayesian restoration of images. *IEEE Trans. Pattern Analysis, and Machine Intelligence*, 6:721–741.
- Gomez-Lopera, J.F., Martinez-Aroza, J., Robles-Perez, A.M., and Roman-Roldan, R. 2000. An analysis of edge detection by using the jensen-shannon divergence. *J. Mathematical Imaging and Vision*, 13:35–56.
- Grenander, U. and Srivastava, A. 2001. Probability models for clutter in natural images. *IEEE Trans. Pattern Analysis, and Machine Intelligence*, 23(4):424–429.
- He, Y., Hamza, A.B., and Krim, H. 2003. A generalized divergence measure for robust image registration. *IEEE Trans. Signal Process.*, 51.
- Hyvarinen, A. 1997. New approximations of differential entropy for independent component analysis and projection pursuit. Tech. Rep., Helsinki University of Technology.
- Hyvarinen, A. and Oja, E. 2000. Independent component analysis: Algorithms and applications. *Neural Networks*, 13(4–5):411–430.
- Imai, H. and Iri, M. 1986. Computational-geometric methods for polygonal approximations of a curve. *Computer Vision, Graphics, and Image Processing*, 36:31–41.
- Jain, A.K. and Farrokhnia, F. 1991. Unsupervised texture segmentation using Gabor filters. *Pattern Recognition*, 24(12):1167–1186.
- Jaynes, E.T. 1963. *Information Theory and Statistical Mechanics*. K. Ford (Ed.), New York, p. 181.
- Kass, M., Witkin, A., and Terzopoulos, D. 1988. Snakes: Active contour models. *Int. J. Computer Vision*, 1(4):321–331.
- Kendall, M. and Stuart, A. 1958. *The Advanced Theory of Statistics*. Charles Griffin & Company.
- Kichenassamy, S., Kumar, A., Olver, P., Tannenbaum, A., and Yezzi, A. 1995. Gradient flows and geometric active contours. In *Proc. Int. Conf. on Computer Vision*, pp. 810–815.
- Koch, M.W. and Kashyap, R.L. 1987. Using polygons to recognize and locate partially occluded objects. *IEEE Trans. Pattern Analysis, and Machine Intelligence*, 9(4):483–494.
- Kurozumi, Y. and Davis, W.A. 1982. Polygonal approximation by the minimax method. *Comput. Graph., Image Proc.*, 248–264.
- Leclerc, Y. 1989. Constructing stable descriptions for image partitioning. *Int. J. Computer Vision*, 3:73–102.
- Lin, J. 1991. Divergence measures based on the Shannon entropy. *IEEE Trans. Information Theory*, 37(1):145–151.
- Malladi, R., Sethian, J.A., and Vemuri, B.C. 1995. Shape modeling with front propagation: A level set approach. *IEEE Trans. Pattern Analysis, and Machine Intelligence*, 17(2):158–173.
- Manjunath, B.S. and Chellappa, R. 1991. Unsupervised texture segmentation using Markov Random Field models. *IEEE Trans. Pattern Analysis, and Machine Intelligence*, 13(5):478–482.
- Mumford, D. and Shah, J. 1985. Boundary detection by minimizing functionals. In *Proc. IEEE Conf. on Computer Vision and Pattern Recognition*, San Francisco.
- O’Connell, K.J. 1997. Object-adaptive vertex-based shape coding method. *IEEE Trans. Circuits and Systems on Video Technology*, 7:251–255.
- Osher, S. and Sethian, J.A. 1988. Fronts propagating with curvature dependent speed: Algorithms based on the Hamilton-Jacobi formulation. *J. Computational Physics*, 49:12–49.
- Paragios, N. and Deriche, R. 2002. Geodesic active regions and level set methods for supervised texture segmentation. *Int. J. Computer Vision*, 46(3):223–247.
- Ronfard, R. 1994. Region-based strategies for active contour models. In *IJCV*, 13:229–251.
- Sethian, J.A. 1999. *Level Set Methods and Fast Marching Methods*. Cambridge University Press.
- Siddiqi, K., Lauziere, Y.B., Tannenbaum, A., and Zucker, S.W. 1998. Area and length minimizing flows for shape segmentation. *IEEE Trans. Image Process.*, 7(3):433–443.
- Simoncelli, E.P., Freeman, W.T., Adelson, E. H., and Heeger, D.J. 1992. Shiftable multiscale transforms. *IEEE Trans. Information Theory*, 38(2):587–607.
- Tsai, A., Yezzi, A., and Willsky, A. 2001. Curve evolution implementation of the Mumford-Shah functional for image

- segmentation, denoising, interpolation, and magnification. *IEEE Trans. Image Process.*, 10(8):1169–1186.
- Ulaby, F.T. 1997. *Fundamentals of Applied Electromagnetics*. Prentice Hall, New Jersey.
- Unal, G., Krim, H., and Yezzi, A. 2002. Active polygons for object tracking. In *IEEE 1st Int. Conf. 3D Data Processing and Visualization and Transmission*, Padova, Italy.
- Yezzi, A., Tsai, A., and Willisky, A. 1999. A statistical approach to snakes for bimodal and trimodal imagery. In *Proc. Int. Conf. on Computer Vision*, pp. 898–903.
- Yezzi, A., Tsai, A., and Willisky, A. 2002. A fully global approach to image segmentation via coupled curve evolution equations. *Journal of Visual Communication and Image Representation*, 13(1):195–216.
- Yun, B.-J., Lee, S.-W., and Kim, S.-D. 2001. Vertex adjustment method using geometric constraint for polygon-based shape coding. *Electronics Letters*, 37:754–755.
- Zhu, S. and Yuille, A. 1996. “Region competition: Unifying snakes, region growing, and Bayes/MDL for multiband image segmentation.” *IEEE Trans. Pattern Analysis, and Machine Intelligence*, 18:884–900.
- Zhu, S.C., Wu, Y., and Mumford, D. 1998. Filters, random fields and maximum entropy (FRAME): Towards a unified theory for texture modeling. *Int. J. Computer Vision*, 27(2):107–126.